Living Around Active Stars
Proceedings IAU Symposium No. 328, 2016
D. Nandy, A. Valio & P. Petit, eds.

doi:10.1017/S1743921317004276

The solar proxy κ^1 Cet and the planetary habitability around the young Sun

J.-D. do Nascimento, Jr.[1,2], A. A. Vidotto[3,4], P. Petit[5], C. Folsom[6], G. F. Porto de Mello[7], S. Meibom[2], X. C. Abrevaya[8], I. Ribas[9], M. Castro[1], S. C. Marsden[10], J. Morin[11], S. V. Jeffers[12], E. Guinan[13] and Bcool Collaboration

[1]Univ. Federal do Rio G. do Norte, UFRN, Dep. de Fisica, CP 1641, 59072-970, Natal, RN, Brazil: jdonascimento@fisica.ufrn.br
[2]Harvard-Smithsonian Center for Astrophysics, 60 Garden Street, Cambridge MA 02138, US
[3]Observatoire de Genève, 51 ch. des Maillettes, CH-1290, Switzerland
[4]School of Physics, Trinity College Dublin, Dublin 2, Ireland
[5]Univ. de Toulouse, UPS-OMP, IRAP, CNRS, 14 Av. E. Belin, F-31400 Toulouse, France
[6] Univ. Grenoble Alpes, IPAG, F-38000 Grenoble, France
[7]Observ. do Valongo, UFRJ, L do Pedro Antoio,43 20080-090, RJ, Brazil
[8] Inst. de Astronom y Fica del Espacio (IAFE), UBA CONICET, Buenos Aires, Argentina
[9]Inst. de Ciències de l'Espai, C. de Can Magrans, s/n, Campus UAB, 08193 Bellaterra, Spain
[10]CESCR, Univ. of Southern Queensland, Toowoomba, 4350, Australia
[11]LUPM-UMR5299, U. Montpellier, Montpellier, F-34095, France
[12]I. für Astrophysik, G.-August-Univ., D-37077, Goettingen, Germany
[13]Univ. of Villanova, Astron. Department, PA 19085 Pennsylvania, US

Abstract. Among the solar proxies, κ^1 Cet, stands out as potentially having a mass very close to solar and a young age. We report magnetic field measurements and planetary habitability consequences around this star, a proxy of the young Sun when life arose on Earth. Magnetic strength was determined from spectropolarimetric observations and we reconstruct the large-scale surface magnetic field to derive the magnetic environment, stellar winds, and particle flux permeating the interplanetary medium around κ^1 Cet. Our results show a closer magnetosphere and mass-loss rate 50 times larger than the current solar wind mass-loss rate when Life arose on Earth, resulting in a larger interaction via space weather disturbances between the stellar wind and a hypothetical young-Earth analogue, potentially affecting the habitability. Interaction of the wind from the young Sun with the planetary ancient magnetic field may have affected the young Earth and its life conditions.

Keywords. Kappa 1 Ceti, HD 20630, solar analog, magnetic field, winds, outflows, habitability

1. Introduction

Large-scale surface magnetic fields measurements of a young Sun proxy from Zeeman Doppler imaging (ZDI) techniques (Semel 1989; Donati *et al.* 2006) give us crucial information about the early Sun's magnetic activity, and today, thanks to spectropolarimetric observations we can reconstruct the magnetic field topology of the stellar photosphere and provide quantitatively the interactions between the stellar wind and the surrounding planetary system. For understanding the origin and evolution of life on Earth we need to know the evolution of the Sun itself, especially the early evolution of its radiation field, particle and magnetic properties. The irradiation from the central star is, by far, the most important source of energy in planetary atmospheres. The radiation field defines the habitable zone, a region in which orbiting planets could sustain liquid water at their surface (Huang 1960; Kopparapu *et al.* 2013). The magnetic environment (and particles)

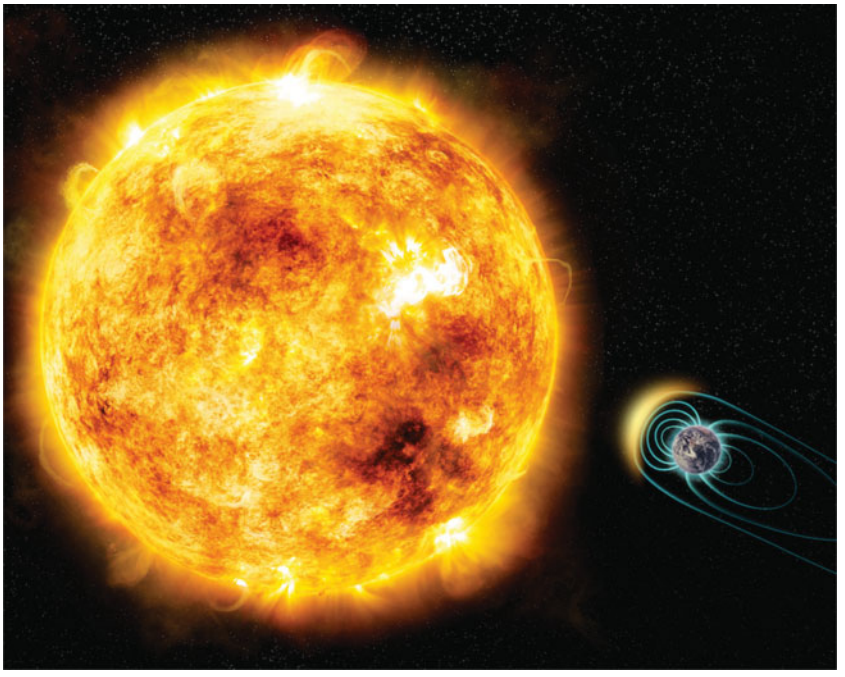

Figure 1. Artist's illustration of the young Sun-like star κ^1 Cet blotched with large starspots, a sign of its high level of magnetic activity and an Earth-like planet with magnetic field protecting its atmosphere and habitability. The physical sizes of the star and planet and distance between them are not to scale. Copyright M. Weiss/CfA-Harvard Smithsonian and do Nascimento *et al.* (2016).

define the interactions star – planet. In the case of magnetized planets, such as the Earth that developed a magnetic field at least four billion years ago (Tarduno *et al.* 2015), their magnetic fields act as obstacles to the stellar wind, deflecting it and protecting the upper planetary atmospheres and ionospheres against the direct impact of stellar wind plasmas and high-energy particles (Kulikov *et al.* 2007; Lammer *et al.* 2007). Focused on carefully selected and well-studied stellar proxies that represent key stages in the evolution of the Sun, The Sun in Time program from Dorren & Guinan (1994), Ribas *et al.* (2005), studied a small sample in the X-ray, EUV, and FUV domains. However, nothing or little has been done in this program with respect to the magnetic field properties for those stars. A characterization of a genuine young Sun proxy is a difficult task, because ages for field stars, particularly for those on the bottom of the main sequence are notoriously difficult to be derived (e.g., do Nascimento *et al.* 2014). Fortunately, stellar rotation rate for young low mass star decrease with time as they lose angular momenta. This rotation rates give a relation to determine stellar age (Kawaler 1989; Barnes 2007; Meibom *et al.* 2015). Young solar analogue stars rotate faster than the Sun and show a much higher level of magnetic activity with highly energetic flares. This behavior is driven by the dynamo mechanism, which operates in rather different regimes in these young objects.

2. κ^1 Cet spectropolarimetric observations and measurements

Find a star that faithfully represents the young Sun in terms of age, mass and metallicity is not an easy task. Kappa 1 Ceti (HD 20630, HIP 15457) is a solar proxy studied by the Sun in Time program. A nearby G5 dwarf star with V = 4.85 and age from 0.4

https://doi.org/10.1017/S1743921317004276 Published online by Cambridge University Press

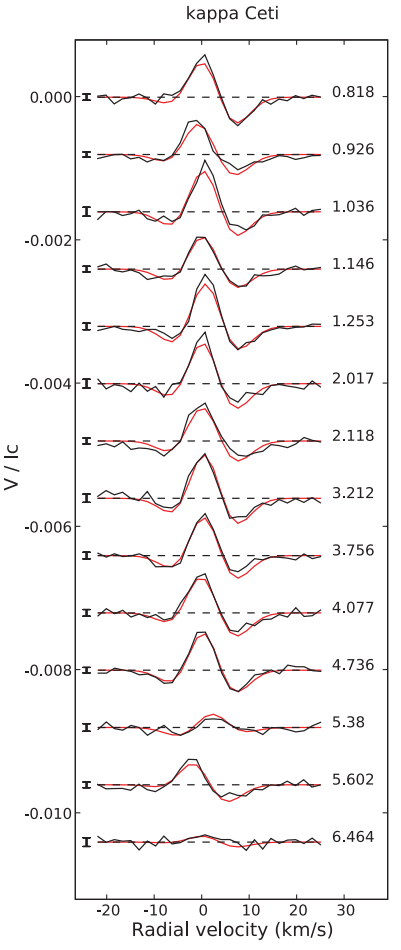

Figure 2. The normalized Stokes V LSD profiles time series of κ^1 Cet. Continuum black lines represent observed profiles and red lines correspond to synthetic profiles of our model. Successive profiles are shifted vertically for display clarity. Rotational cycle is shown on the right of each profile. 1 σ error bars for each observation are indicated on the left of each rotational phase (calculated by assuming a rotation period of 9.2 d, and a reference Julian date arbitrary set to 2456195.0). Horizontal dashed lines illustrate the zero levels of each observation (do Nascimento *et al.* 2016).

Gyr to 0.6 Gyr (Ribas *et al.* 2010) that stands out potentially having a mass very close to solar and age of the Sun when the window favorable to the origin of life opened on Earth around 3.8 Gyr ago or earlier (Mojzsis *et al.* 1996). This corresponds to the period when favorable physicochemical and geological conditions became established and after the late heavy bombardment. As to the Sun at this stage, κ^1 Cet radiation environment determined the properties and chemical composition of the close planetary atmospheres, and provide an important constraint of the role played by the Earth magnetospheric protection at the critical time at the start of the Archean epoch (Mojzsis *et al.* 1996), when life is thought to have originated on Earth. This is also the epoch when Mars lost its liquid water inventory at the end of the Noachian epoch some 3.7 Gyr ago (Jakosky *et al.* 2001). Study based on κ^1 Cet can also clarify the biological implications of the high-energy particles at this period (Cnossen *et al.* 2008) and add straight constraints limiting the possibility of lithopanspermia process on the Mars-Earth system (Abrevaya

https://doi.org/10.1017/S1743921317004276 Published online by Cambridge University Press

2016). Such a studies require careful analysis based on reasonably bright stars at specific evolutionary state, and there are only a few number of bright solar analogues at this age of κ^1 Cet. The Figure 1 represents an artistic illustration of the young Sun-like star κ^1 Cet blotched with large starspots, a sign of its high level of magnetic activity. Physical sizes of the star and planet and distance between them are not to scale.

Spectropolarimetric data of κ^1 Cet were collected with the NARVAL spectropolarimeter (Aurière 2003) at the 2.0-m Bernard Lyot Telescope (TBL) of Pic du Midi Observatory as part of TBL Bcool Large Program (Marsden *et al.* 2014). NARVAL comprises a Cassegrain-mounted achromatic polarimeter and a bench-mounted cross-dispersed echelle spectrograph. In polarimetric mode, NARVAL has a spectral resolution of about 65,000 and covers the whole optical domain in one single exposure, with nearly continuous spectral coverage ranging from 370 nm to 1000 nm over 40 grating orders. The data reduction is performed through Libre-ESpRIT package based on ESPRIT (Donati *et al.* 1997). As described by do Nascimento *et al.* (2016), Stokes I and V (circularly-polarized) spectra were gathered. The resulting time-series is composed of 14 individual observations collected over 53 consecutive nights, during which more than one rotation period (assuming a rotation period of 9.2 d). As usually for cool active stars, Stokes V spectra do not display any detectable signatures in the individual spectral lines, even with a peak S/N in excess of 1,000 (at wavelengths close to 730 nm). In this situation, we take advantage of the fact that, at first order, Stokes V Zeeman signatures of different spectral lines harbor a similar shape and differ only by their amplitude, so that a multiline approach in the form of a cross-correlation technique is able to greatly improve the detectability of tiny polarized signatures. We employ here the Least-Squares-Deconvolution method (LSD, Donati *et al.* 1997; Kochukhov 2010) using a procedure similar to the one described in Marsden *et al.* (2014). Our line-list is extracted from the VALD data base (Kupka *et al.* 2000) and is computed for a set of atmospheric parameters (effective temperature and surface gravity) similar to those of κ^1 Cet. We assume a total of about 8,400 spectral lines recorded in NARVAL spectra and listed in our line mask, the final S/N of Stokes V LSD pseudo-profiles is ranging from 16,000 to 28,000, well enough to detect Zeeman signatures at all available observations (Figure 2). From the Stokes I spectra, we also determined the S_{index}, calibrated from the Mount Wilson S_{index}, to quantify the chromospheric emission changes in the Ca II H line (do Nasciemento *et al.* 2014). The complete pipeline of the S_{index} computation is described in Morgenthaler *et al.* (2012) and Wright *et al.* (2004).

3. Fundamental parameters and evolutionary status

Based on our NARVAL data we performed spectroscopic analysis of κ^1 Cet to redetermine stellar parameters as in do Nascimento *et al.* (2013) and references therein. We used excitation and ionization equilibrium of a set of 209 Fe I and several Fe II lines and an atmosphere model and mostly laboratory gf-values to compute a synthetic spectra. The best solution from this synthetic analysis was fitted to the NARVAL spectrum for the set of parameters $T_{\rm eff}$ = 5705 ± 50 K, [Fe/H] = +0.10 ± 0.05 dex, log g = 4.49 ± 0.10. Several photometric and spectroscopic observational campaigns were carried out to determine κ^1 Cet fundamental parameters. Ribas *et al.* (2010) determined the photometric $T_{\rm eff}$ of κ^1 Cet from intermediate-band Strömgren photometry, based on the 2MASS near-IR photometry and a fit of the spectral energy distribution with stellar atmosphere models. This photometric method yielded $T_{\rm eff}$ = 5685 ± 45 K. Ribas *et al.* (2010) also determined spectroscopic fundamental parameters of κ^1 Cet as $T_{\rm eff}$ = 5780 ± 30 K, log g = 4.48 ± 0.10 dex, [Fe/H] = +0.07 ± 0.04 dex. Valenti & Fischer (2005) gives $T_{\rm eff}$ = 5742 K, log g = 4.49 dex, [M/H] = +0.10 dex. Paletou *et al.* (2015), from high resolution

https://doi.org/10.1017/S1743921317004276 Published online by Cambridge University Press

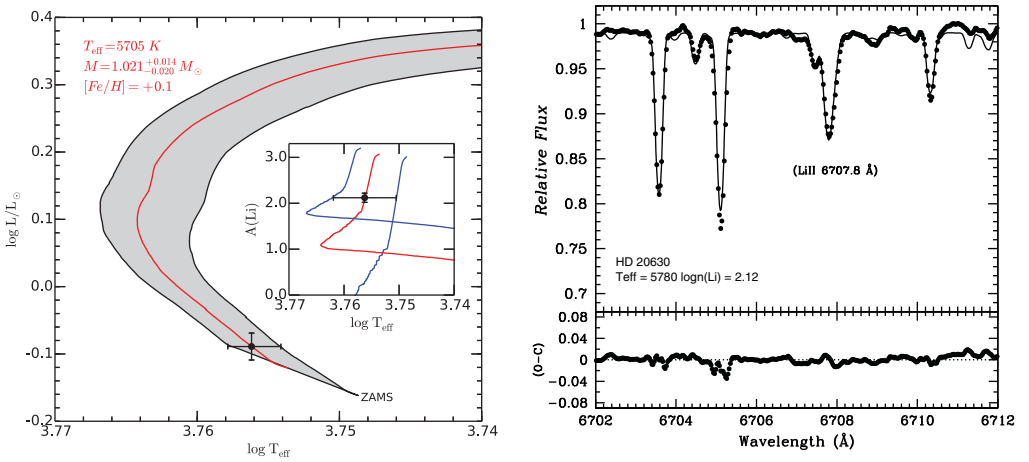

Figure 3. The **left painel**, κ^1 Cet in the Hertzsprung-Russell diagram. Luminosities and related errors have been derived from the Hipparcos parallaxes. The typical errors on Teff are from our spectroscopic analysis. The shaded zone represents the range of masses in TGEC models (the maximum and the minimum masses are indicated) limited by the 1σ observational error bars. The inside plot shows the lithium destruction for κ^1 Cet along the evolutionary tracks as a function of the effective temperature. The blue tracks represent the range of masses of TGEC models (the maximum and the minimum masses) limited by the 1σ observational error bars. The **right painel**, Spectral synthesis of the λ 6707 Li I line of κ^1 Cet based on spectroscopic set of atmospheric parameters as described by Ribas *et al.* (2010). The derived abundance logN(Li) = 2.12, in the usual scale where logN(H) = 12.00. This value is in good agreement with the determinations of Luck & Heiter (2006) and Pasquini *et al.* (1994)

NARVAL Echelle spectra (R = 65,000, S/N $\sim$ 1000) described in the Sect. 2, determined $T_{\rm eff}$ = 5745 $\pm$ 101 K, log g = 4.45 $\pm$ 0.09 dex, [Fe/H] = +0.08 $\pm$ 0.11. Spectroscopic $T_{\rm eff}$ values are hotter than photometric, and a possible explanation of this offset could be effects of high chromospheric activity and, an enhanced non-local UV radiation field resulting in a photospheric overionization (Ribas *et al.* 2010). The presented spectroscopic $T_{\rm eff}$ values are in agreement within the uncertainty. Finally we used our determined solution $T_{\rm eff}$ = 5705 $\pm$ 50 K, [Fe/H] = +0.10 $\pm$ 0.05 dex, log g = 4.49 $\pm$ 0.10. This yields a logN(Li) = 2.05, in good agreement with logN(Li) = 2.12 determined by Ribas *et al.* (2010) and presented in the Figure 3 right. To constrain the evolutionary status of κ^1 Cet, we used the spectroscopic solution within computed models with the Toulouse-Geneva stellar evolution code (do Nascimento *et al.* 2013). We used models with an initial composition from Grevesse & Noels (1993). Transport of chemicals and angular momentum due to rotation-induced mixing are computed as described in Vauclair & Théado (2003) and presented in the Figure 3 left. The angular momentum evolution follows the Kawaler (1988) prescription. We calibrated a solar model as Richard *et al.* (1996) and used this calibration to compute κ^1 Cet model. These models, together with lithium abundance measurement, result in mass of 1.02 $\pm$ 0.02 $M_\odot$, an age between 0.5 Gyr to 0.9 Gyr for κ^1 Cet, consistent with Güdel *et al.* (1997) estimated age of 0.75 Gyr and Marsden *et al.* (2014) estimated age of 0.82 Gyr using our data and activity-age calibration.

For rotation period $P_{\rm rot}$, as in do Nascimento *et al.* (2014), we measured the average surface $P_{\rm rot}$ from light curves. Here, for κ^1 Cet we used MOST (Microvariability and Oscillations of Stars) (Walker *et al.* 2003) light curve modulation (Figure 4). MOST continuously observed κ^1 Cet for weeks at a time providing a $P_{\rm rot}$ (Walker *et al.* 2003). We extract $P_{\rm rot}$ from Lomb–Scargle periodogram (Scargle 1982) and a wavelet analysis of the light curve (Figure 4). The $P_{\rm rot}$ obtained was $P_{\rm rot}$ = 8.77d $\pm$ 0.8 days, three

https://doi.org/10.1017/S1743921317004276 Published online by Cambridge University Press

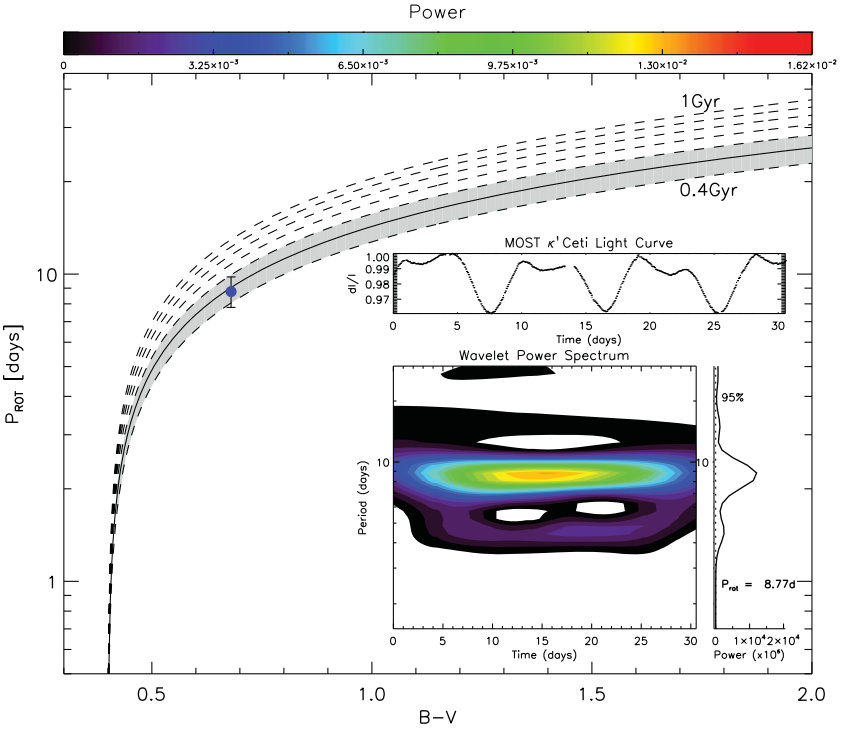

Figure 4. Colour–period diagram for κ^1 Cet based on $P_{\rm rot}$ measurement from MOST (Microvariability and Oscillations of Stars) light curve. Lomb–Scargle periodogram (Scargle 1982) and wavelet (inside figure) was used to derive rotation period. The predictions from gyrochronology models (Barnes 2007) of cool star are plotted for different ages.

times shorter than the solar $P_{\rm rot}$. The $P_{\rm rot}$ we have measured from the *MOST* light curves allows us an independent (from classical isochrone) age derivation of κ^1 Cet using gyrochronology (Skumanich 1972; Barnes 2007). The gyrochronology age of κ^1 Cet that we derive range from 0.4 Gyr to 0.6 Gyr (Figure 4), consistent with the predictions from Ribas *et al.* (2010) and ages determined from evolutionary tracks.

4. κ^1 Cet Magnetic field topology

Our implementation of the ZDI algorithm is the one detailed by Donati *et al.* (2006), where the surface magnetic field is projected onto a spherical harmonics frame. From the time-series of Stokes V profiles, we used the ZDI method (Zeeman-Doppler Imaging, Semel 1989) to reconstruct the large-scale magnetic topology of the star. We assume during reconstruction a projected rotational velocity equal to 5 km/s (Valenti & Fischer 2005), a radial velocity equal to 19.1 km/s, and an inclination angle of 60 degrees (from the projected rotational velocity, radius and stellar rotation period). We truncate the spherical harmonics expansion to modes with $l \leqslant 10$ since no improvement is noticed in our model if we allow for a more complex field topology. Given the large time-span of our observations, some level of variability is expected in the surface magnetic topology. A fair amount of this intrinsic evolution is due to differential rotation, which can be taken into account in our inversion procedure assuming that the surface shear obeys a simple law of the form $\Omega(l) = \Omega_{\rm eq} - \sin^2(l) d\Omega$, where $\Omega(l)$ is the rotation rate at latitude l, $\Omega_{\rm eq}$ is the rotation rate of the equator and $d\Omega$ is the difference of rotation rate between the

https://doi.org/10.1017/S1743921317004276 Published online by Cambridge University Press

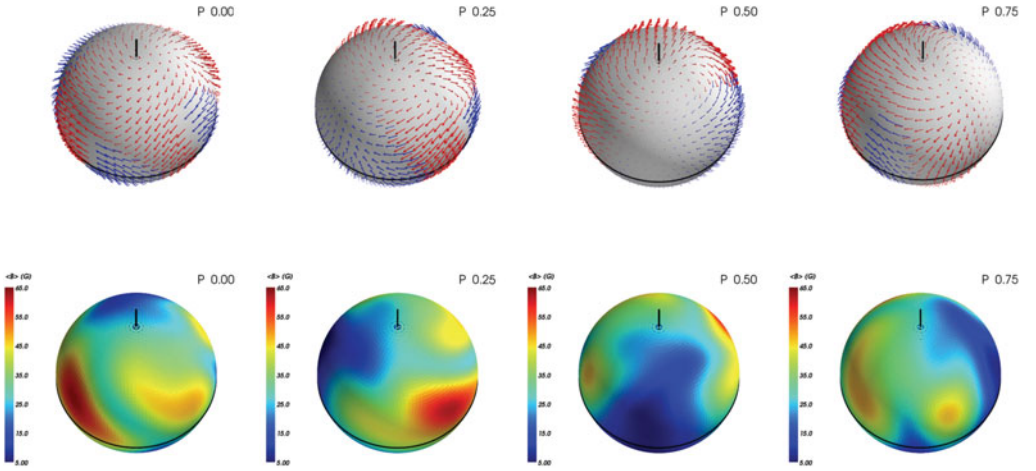

Figure 5. Large-scale magnetic topology of κ^1 Cet at different rotation phases indicated in the top right of each panel. The top row shows the inclination of field lines over stellar surface, with red and blue arrows depicting positive and negative field radial component values, respectively. The bottom row displays the field strength (do Nascimento *et al.* 2016).

pole and the equator. We optimize the two free parameters $\Omega_{\rm eq}$ and $d\Omega$ by computing a 2D grid of ZDI models spanning a range of values of these two parameters, following the approach of (Petit *et al.* 2002). By doing so, we obtain a minimal reduced χ^2 equal to 1.3 at $\Omega_{\rm eq} = 0.7$ rad/d and $d\Omega = 0.056$ rad/d. These values correspond to a surface shear roughly solar in magnitude, with an equatorial rotation period $P_{\rm rot}^{\rm eq} = 8.96$ d, while the polar region rotates in about $P_{\rm rot}^{\rm pole} = 9.74$ d. Figure 5 from top to bottom presents the inclination of field lines over the stellar surface and the resulting large-scale magnetic geometry. The surface-averaged field strength is equal to 24 G, with a maximum value of 61 G at phase 0.1. A majority (61%) of the magnetic energy is stored in the toroidal field component, showing up as several regions with field lines nearly horizontal and parallel to the equator, e.g. at phase 0.1. The dipolar component of the field contains about 47% of the magnetic energy of the *poloidal* field component, but significant energy is also seen at $\ell > 3$, where 20% of the magnetic energy is reconstructed. Axisymmetric modes display 66% of the total magnetic energy. These magnetic properties are rather typical of other young Sun-like stars previously observed and modeled with similar techniques (Petit *et al.* 2008, Folsom *et al.* 2016 and references therein).

5. Stellar wind and effects on the magnetosphere of the young Earth

We reconstruct the κ^1 Cet large-scale surface magnetic field based on spectropolarimetric observations and we derive the magnetic environment and particle flux permeating the interplanetary medium around κ^1 Cet. Stellar winds are is an important point, and we use here that one presented in Vidotto *et al.* (2012, 2015), in which we use the three-dimensional magnetohydrodynamics (MHD) numerical code BATS-R-US (Powell *et al.* 1999; Tóth *et al.* 2012) to solve the set of ideal MHD equations. In this model, as described in do Nascimento *et al.* (2016), we use, as inner boundary conditions for the stellar magnetic field, the radial component of the reconstructed surface magnetic field of κ^1 CetẆe assume the wind is polytropic, with a polytropic index of $\gamma = 1.1$, and consists of a fully ionised hydrogen plasma. We further assume a stellar wind base density of 10^9 cm^{-3} and a base temperature of 2 MK. Figure 5 shows the large-scale

https://doi.org/10.1017/S1743921317004276 Published online by Cambridge University Press

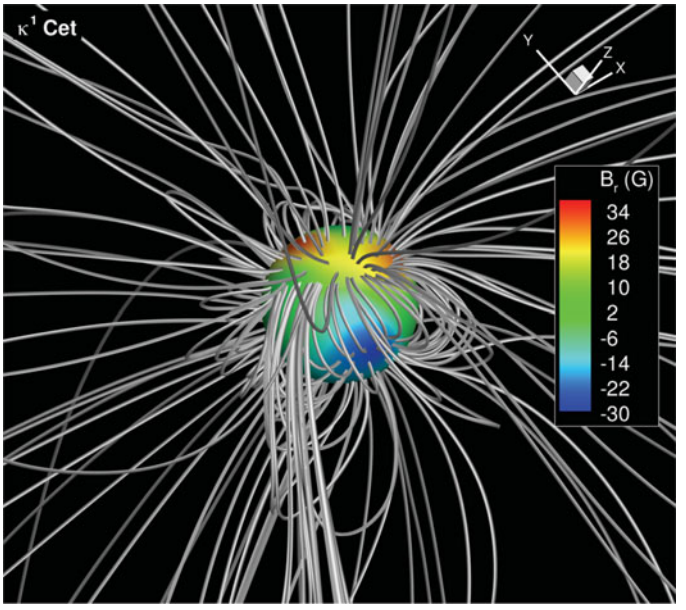

Figure 6. Large-scale magnetic field embedded in the wind of κ^1 Cet. The radial component of the observationally reconstructed surface magnetic field is shown in colour.

magnetic field embedded in the wind of κ^1 Cet. In our model, we derive a mass-loss rate of $\dot{M} = 9.7 \times 10^{-13}$ $M_\odot$ yr^{-1}, i.e., almost 50 times larger than the current solar wind mass-loss rate. It is interesting to compare our results to the empirical correlation between $\dot{M}$ and X-ray fluxes (F_X) derived by Wood *et al.* (2014). For κ^1 Cet, the X-ray luminosity is $10^{28.79}$ erg/s (Wood *et al.* 2012). Assuming a stellar radius of $0.95R_\odot$, we derive $F_X \simeq 10^6$ erg cm^{-2} s^{-1} and, according to Wood *et al.* (2012) relation, $\dot{M}$ to be ~ 63 to 140 times the current solar wind mass-loss rate. Thus, our $\dot{M}$ derivation roughly agrees with the lower envelope of the empirical correlation of Wood *et al.* (2014) and derived mass-loss rate of Airapetian & Usmanov (2016).

5.1. *The mass-loss rate of the young Sun*

The enhanced mass-loss rate of the young solar analogue κ^1 Cet implies that the strengths of the interactions between the stellar wind and a hypothetical young-Earth analogue is larger than the current interactions between the present-day solar wind and Earth. To quantify this, we calculate the ram pressure of the wind of κ^1 Cet as $P_{\rm ram} = \rho u^2$, where ρ is the particle density and u the wind velocity (Figure 7). Pressure balance between the magnetic pressure of a hypothetical young-Earth and the ram pressure of the young Sun's wind allows us to estimate the magnetospheric size of the young-Earth:

$$\frac{r_M}{R_\oplus} = f \left(\frac{B_{\rm eq,\oplus}^2}{8\pi P_{\rm ram}} \right)^{1/6} \tag{5.1}$$

where $B_{\rm eq,\oplus}$ is the equatorial field strength of the young Earth dipolar magnetic field and $f \simeq 2^{2/6}$ is a correction factor used to account for the effects of currents (e.g., Cravens 2004). Figure 8a shows the stand-off distance of the Earth's magnetopause calculated using Eq. (5.1). Here, we assume three values for $B_{\rm eq,\oplus}$: (i) $B_{\rm eq,\oplus} = 0.31$G, identical to the present-day magnetic field strength (e.g., Bagenal 1992); (ii) $B_{\rm eq,\oplus} = 0.15$G, according

https://doi.org/10.1017/S1743921317004276 Published online by Cambridge University Press

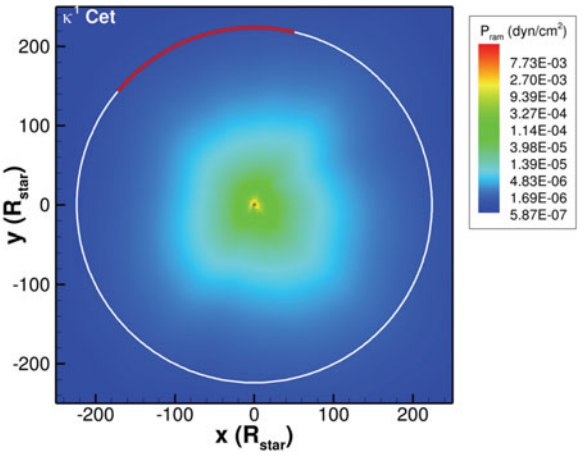

Figure 7. The ram pressure of the stellar wind of κ^1 Cet. The circle indicates the position of the orbit of a young-Earth analogue. Red portions of the orbit indicates regions of negative vertical component of the interplanetary magnetic field ($B_z < 0$).

to measurements of the Paleoarchean Earth's magnetic field (3.4Gyr ago) (Tarduno *et al.* 2010); and (iii) $B_{\mathrm{eq},\oplus} = 0.40$G, according to rotation-dependent dynamo model theory (see Sterenborg *et al.* 2011). Depending on the assumed field strength of the hypothetical young-Earth, the average magnetospheric sizes are (i) $4.8R_\oplus$, (ii) $3.8R_\oplus$ and (iii) $5.3R_\oplus$, respectively, indicating a size that is about 34 to 48% the magnetospheric size of the present-day Earth (about $11R_\oplus$, (Bagenal 1992).

The relative orientation of the interplanetary magnetic field with respect to the orientation of the planetary magnetic moment plays an important role in shaping the open-field-line region (polar cap) of the planet (e.g., Sterenborg *et al.* 2011). Through the polar cap, particles can be transported to/from the interplanetary space. Tarduno *et al.* (2010) discusses that the increase in polar cap area should be accompanied by an increase of the volatile losses from the exosphere, which might affect the composition of the planetary atmosphere over long timescales. In the case where the vertical component of interplanetary magnetic field B_z is parallel to the planet's magnetic moment (or anti-parallel to the planetary magnetic field at r_M), the planetary magnetosphere is in its widest open configuration and a polar cap develops. If B_z and the planet's magnetic moment are anti-parallel, there is no significant polar cap. The complex magnetic-field topology of κ^1 Cet gives rise to non-uniform directions and strengths of B_z along the planetary orbit. The red (white) semi-circle shown in Figure 7 illustrates portions of the orbital path surrounded by negative (positive) B_z. Therefore, depending on the relative orientation between B_z and the planet's magnetic moment, the colatitude of the polar cap will range from 0^o (closed magnetosphere) to $\arcsin(R_\oplus/r_M)^{1/2}$ (widest open configuration) (e.g., Vidotto *et al.* 2013). Figure 8b shows the colatitude of the polar cap for the case where the planetary magnetic moment points towards positive z. Portions of the orbit where the planet is likely to present a closed magnetosphere (from 76 to 140 degrees in longitude) are blanked out.

6. Conclusions

We report a magnetic field detection for κ^1 Cet with an average field strength of 24 G, and maximum value of 61 G. The complex magnetic-field topology of κ^1 Cet gives rise

https://doi.org/10.1017/S1743921317004276 Published online by Cambridge University Press

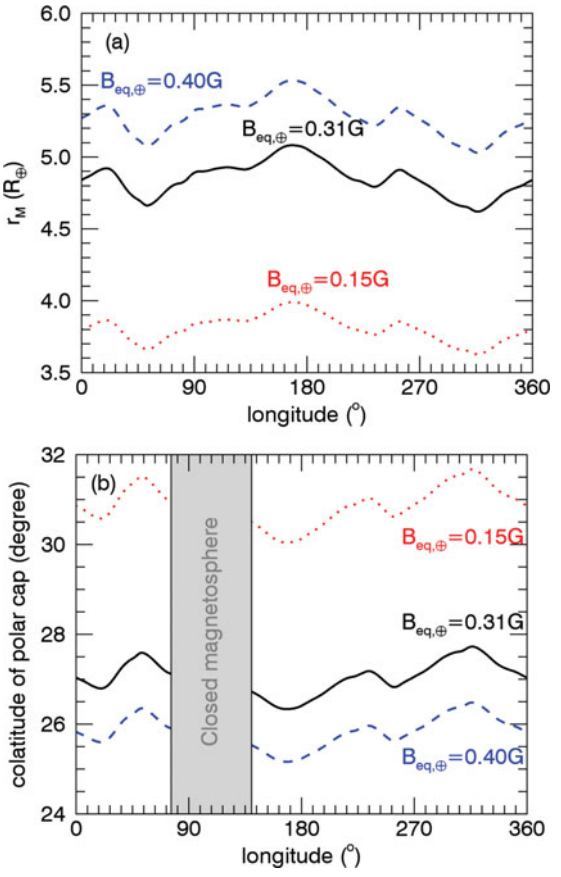

Figure 8. (a) The magnetospheric size of the young-Earth is calculated through pressure balance between the ram pressure of the young Sun's wind (Figure 7) and the magnetic pressure of the planetary magnetosphere for different equatorial dipolar field strengths. (b) The related colatitude of the polar cap, assuming that during most of the orbit, the planetary magnetic moment is parallel to the interplanetary magnetic field.

to non-uniform directions and strengths along a possible planetary orbit. Our stellar wind model for κ^1 Cet shows a mass-loss rate factor 50 times larger than the current solar wind mass-loss rate, resulting in a larger interaction between the stellar wind and a hypothetical young-Earth like planet. With 1.02 $M_\odot$, an age between 0.4 Gyr to 0.6 Gyr, κ^1 Cet is a perfect target to study habitability on Earth during the early Sun phase when life arose on Earth. An enhanced mass-loss, high-energy emissions from κ^1 Cet, supporting the extrapolation from Newkirk (1980) and Lammer *et al.* (2007) of a Sun with stronger activity 3.8 Gyr ago or earlier. Early magnetic field have affected the young Earth and its life conditions and due to the ancient magnetic field on Earth four billion years ago as measured by Tarduno *et al.* (2015), the early magnetic interaction between the stellar wind and the young-Earth planetary magnetic field may well have prevented the volatile losses from the Earth exosphere and create conditions to support life. κ^1 Cet magnetic field strength and wind mass-loss rate tell us that life at the primitive Earth surface 3.8 Gyr have been exposed to a higher radiation level, when compared to present time.

https://doi.org/10.1017/S1743921317004276 Published online by Cambridge University Press

References

Abrevaya, X. C. 2017, *Living around active stars. Proceedings of IAU Symposium 328.*

Airapetian V. S. & Usmanov A. V. 2016, *ApJL*, 817, 24

Aurière, M. 2003, in Arnaud J., Meunier N. *eds., Magnetism and Activity of the Sun and Stars, EAS Pub. Ser.*, 9, 105

Bagenal, F. 1992, *Annual Review of Earth and Planetary Sciences*, 20, 289

Barnes, S. A. 2007, *ApJ*, 669, 1167

Cravens, T. E. 2004, *Physics of Solar System Plasmas*

Cnossen, I., Sanz-Forcada, J., Favata, F., Witasse, O., Zegers, T., & Arnold, N. F. 2007, *J. Geophys. Res. (Planets)*, 112, 2008

Dorren, J. D. & Guinan, E. F. 1994, *IAU 143, The Sun as a Variable Star, ed. J. M. Pap, C. Frölich, H. S. Hudson, & S. Solanki, Cambridge U. Press*, 206

do Nascimento, J. D., Petit, P., Castro, M. *et al.* 2014, *Magnetic Fields throughout Stellar Evolution. Proceedings of the IAU Symposium*, 302, 142

do Nascimento, J. -D., Jr., Takeda, Y., *et al.* 2013, *ApJL*, 771, 31

do Nascimento, J. -D., Jr., García, R. A., *et al.* 2014, *ApJL*, 790, 23

do Nascimento, J. -D., Jr., Vidotto, A. A., *et al.* 2016, *ApJL*, 820, 15

Donati, J.-F., Howarth, I. D., Jardine, M. M. *et al.* 2006, *MNRAS*, 370, 629

Donati, J.-F., Semel, M., Carter, B. D., *et al.* 1997, *MNRAS*, 291, 658

Folsom, C. P., Petit, P., Bouvier, J., *et al.* 2016, *MNRAS*, 457, 580

Grevesse, N. & Noels, A. 1993, *Origin and Evolution of the Elements, eds. N. Prantzos, E. Vangioni–Flam, and M. Cassé, Cambridge U. Press*, 15

Güdel, M., Guinan, E. F., & Skinner, S. L. 1997, *ApJ*, 483, 947

Huang, S.-S. 1960, *Am. Sci.*, 202, 55

Jakosky, B. M. & Phillips, R. J. 2001, *Nature*, 412, 237

Kawaler, S. D. 1988, *ApJ*, 333, 236

Kawaler, S. D. 1989, *ApJ*, 343, L65

Kopparapu, R. K., Ramirez, R., Kasting, J. F., *et al.* 2013, ApJ, 765, 131

Kochukhov, O., Makaganiuk, V., & Piskunov, N. 2010, *A&A*, 524, A5

Kulikov, Y. N., Lammer, H., *et al.* 2007, *Space Sci. Rev.*, 207, 129

Kupka, F. G., Ryabchikova, T. A., Piskunov, N. E., Stempels, H. C., & Weiss W. W. 2000, *Baltic Astronomy*, 9, 590

Lammer, H. *et al.* 2007, *Astrobiology*, 7, 185

Marsden, S. C., Petit, P., *et al.* 2014, *MNRAS*, 4444, 3517

Meibom, S., Barnes, S. A., *et al.* 2015, *Nature*, 517, 589

Mojzsis, S. J., Arrhenius, G., McKeegan, K. D., *et al.* 1996, *Nature*, 384, 55

Morgenthaler, A., Petit, P., Saar, S., Solanki, S. K. *et al.* 2012, *ApJ*, 540, 138

Newkirk, G. 1980, *Geochimica Cosmochimica Acta Suppl.*, 13, 293

Paletou, F., Böhm T., Watson V., & Trouilhet J.-F. 2015, *A&A*, 573, A67

Petit, P., Donati, J.-F., & Collier Cameron, A. 2002, *ApJL*, 771, 31

Petit, P., Dintrans, B., *et al.* 2008, *MNRAS*, 388, 80

Powell, K. G., Roe, P. L., *et al.* 1999, *J. Chem. Phys.*, 154, 284

Ribas, I., Porto de Mello, G. F., Ferreira, L. D., Hebrard, E. *et al.* 2010, *ApJ*, 714, 384

Ribas, I., Guinan, E. F., Güdel, M., & Audard, M. 2005, *ApJ*, 622, 680

Ribas, I., Guinan, E., & Güdel, Audard, M. 2005, *ApJ*, 622, 680

Richard, O., Vauclair, S., *et al.* 1996, *A&A*, 312, 1000

Scargle, J. D. 1982, *ApJ*, 263, 835

Semel, M. 1989, *A&A*, 255, 456

Skumanich, A. 1972, *ApJ*, 171, 565

Sneden, C. 1973, *ApJ*, 184, 839

Sterenborg, M. G., Cohen, O., Drake, J. J., & Gombosi, T. I. 2011, *Journal of Geophysical Research (Space Physics)*, 116, 1217

Tarduno, J. A., Cottrell, R. D., *et al.* 2010, *Science*, 327, 1238

Tarduno, J. A., Cottrell, R. D., *et al.* 2015, *Science*, 349, 521

Tóth, G., van der Holst, B., *et al. 2012*, Journal of Computational Physics, 231, 870
Vauclair, S. & Théado, S. 2003, *A&A*, 587, 777
Valenti, F. A. & Fischer, D. 2005, *ApJS*, 587, 777
Vidotto, A. A., Fares, R., Jardine, M., *et al.* 2012, *MNRAS*, 423, 3285
Vidotto, A. A., Fares, R., Jardine, M., *et al.* 2015, *MNRAS*, 449, 4117
Vidotto, A. A., Jardine, M., Morin, J., *et al.* 2013, *A&A*, 557, A67
Walker, G. A. H., *et al.* 2003, *PASP*, 115, 1023
Wood, B. E., Laming, J. M., & Karovska, M. 2012, *ApJ*, 753, 76
Wright, J. T., Marcy, G. W., Butler, R. P., Vogt, S. S. *et al.* 2004, *ApJS*, 152, 261
Wood, B. E., Müller, H.-R., Redfield, S., & Edelman, E. 2014, *ApJL*, 781, L33

https://doi.org/10.1017/S1743921317004276 Published online by Cambridge University Press